Mechanistic Investigation of a Hybrid Zn/V 2 O 5 Rechargeable Battery with a Binary Li + /Zn 2+ Aqueous Electrolyte

Dauren Batyrbekuly, Sabrina Cajoly, Barbara Laïk, Jean Pierre Pereira-Ramos, Nicolas Emery, Zhumabay Bakenov, Rita Baddour-Hadjean

Mechanistic investigation on hybrid Zn/V_2O_5 rechargeable battery using a binary Li^+/Zn^{2+} aqueous electrolyte

D. Batyrbekuly [1,2], S. Cajoly [1], B. Laïk [1], J-P. Pereira-Ramos [1], N. Emery [1],*

Z. Bakenov [2], R. Baddour-Hadjean [1]

1- Institut de Chimie et des Matériaux Paris Est (ICMPE), UMR 7182 CNRS-Université Paris Est Créteil, 2 rue Henri Dunant, 94320 Thiais, France

2-School of Engineering, National Laboratory Astana, Nazarbayev University, 53 Kabanbay Batyr Avenue, Astana 010000, Kazakhstan

**corresponding author: laik@icmpe.cnrs.fr*

Abstract

Low cost, easy processing and environment-friendly aqueous rechargeable zinc batteries (AZB) have great potential for large-scale energy storage, which justifies they have been receiving extensive attention in recent years. An original concept based on the use of a binary Li^+/Zn^{2+} aqueous electrolyte is described here in the case of Zn/V_2O_5 system. Hybrid means the positive side involves mainly the Li^+ insertion/desinsertion reaction in V_2O_5 while the negative electrode operates according to zinc dissolution-deposition cycles. The Zn // 3 mol L^{-1} Li_2SO_4 – 4 mol L^{-1} $ZnSO_4$ // V_2O_5 cell is working in the narrow 1.6 V - 0.8 V voltage range with interesting capacity values about 136-125 mAh g^{-1} at C/20-C/5 rates respectively. At 1 C, a capacity of 80 mAh g^{-1} is outstandingly stable over more than 300 cycles with a capacity retention of 100 %. A detailed structural study by XRD and Raman spectroscopy allows unravelling the peculiar response of the V_2O_5 layered host lattice upon discharge-charge and cycling. Strong similarities with the well-known structural changes reported in non-aqueous lithiated electrolytes are highlighted, although the emergence of the

usual distorted δ-LiV_2O_5 phase is not detected upon discharge to 0.8 V. The pristine host structure is restored and maintained along cycling with mitigated structural changes leading to the high capacity retention. The present electrochemical and structural findings reveal a reaction mechanism mainly based on Li^+ intercalation, but co-intercalation of a few Zn^{2+} ions between the oxide layers cannot be completely dismissed. The presence of zinc cations between the oxide layers is thought to relieve the structural stress induced in V_2O_5 under operation, resulting in a limited volume expansion of 4 %. These presented fundamental investigations which describe a reaction mechanism operating in an environment-friendly aqueous medium have never been reported in the literature so far.

Keywords:

aqueous Zn hybrid battery (AZB); V_2O_5; environment-friendly aqueous electrolyte; binary Li/Zn electrolyte; reaction mechanism; cycling performance

Introduction

Since a few decades, annual global oil consumption has become greater than the quantities of new deposits discovered. This energy crisis coupled with growing ecological concerns questions everyone about the need for a rapid energy transition, without, however, slowing the ever-increasing need for energy. Such a context involves research on renewable intermittent energies with special attention toward safe and low cost storage solutions.

Non-aqueous Li-ion batteries (LIBs) constitute the best technology for electrochemical energy storage due to their high energy and power density. Leader on the portable electronics market, LIBs are also considered for large scale applications like electric vehicles and stationary grids combined with renewable energies [1]. However, safety aspects due to the flammability of the organic electrolyte as well as cost queries related to the need to use a clean room during the manufacturing process to remove all traces of water are among the crucial points to solve. In recent years, many efforts have been made to develop new concepts to overcome these critical issues. Among them, rechargeable batteries using aqueous electrolytes are attracting considerable attention for electrochemical energy storage [2]. Indeed, besides the environmentally friendly aspect, the non-flammability of the solvent makes them safer. In addition, the use of water-based electrolytes instead of flammable organic electrolytes ensures a high ionic conductivity promoting a high rate capability. Moreover, the total absence of oxygen or moisture being not necessary during preparation, the use of aqueous solvent leads to lower total cost. Naturally, the narrow electrochemical stability window of water, limited at 1.23 V at 25 °C according to thermodynamically considerations, remains a major challenge.

In the last few years, research efforts have intensively focused on Aqueous Zinc Batteries (AZBs) [3–5]. The reasons for this interest are the abundance, low cost and low redox potential (-0.76 V vs. SHE) of Zn, as well as a wide potential range of ~ 2 V due to a high overpotential for hydrogen evolution [6]. Promising data have been reported, namely excellent reversibility and fast kinetics of Zn deposition/dissolution [7] thanks to the use of aqueous electrolytes in neutral or slightly acidic pH preventing Zn dendrites growth [8–10]. On the cathode side, three main groups of active materials have been investigated: Prussian blue and its analogues, manganese compounds and vanadium oxides as well as their derivatives [3,10,11]. Vanadium-based cathodes sparked a great interest due to the rich redox chemistry of vanadium enabling high specific capacities to be reached, and to various open host structures promoting insertion reactions. Attractive results have been recently achieved

with the hydrated $Zn_{0.25}V_2O_5$, nH_2O bronze exhibiting a capacity close to 300 mAh g^{-1}, fast rate capability and long cycle life [4]. From that pioneer work, studies have been extended to hydrated compounds like for instance V_2O_5, nH_2O [12], V_3O_7, H_2O [13], $V_{10}O_{24}$, $12H_2O$ [14], $Mg_xV_2O_5$, nH_2O [15], $K_2V_6O_{16}$, $2.7H_2O$ [16], $Ca_{0.25}V_2O_5$, nH_2O [17], $Na_2V_6O_{16}$, $3H_2O$ [18], $Fe_5V_{15}O_{39}(OH)$, $9.9H_2O$ [19]. Anhydrous phases have also been investigated like VO_2 [20], $Zn_2V_2O_7$ [21], $NH_4V_4O_{10}$ [22], potassium vanadates [23] and LiV_3O_8 [24].

Surprisingly, the pristine conventional V_2O_5 oxide has received less attention compared to its derivatives. Mai's group reported water-free V_2O_5 microplates and, more recently, microspheres performance using a "water-in-salt" electrolyte, mixture of 21 m LiTFSI and 1 m $Zn(CF_3SO_3)$ [25,26], but insertion reaction of cations in this oxide is scarcely reported in conventional aqueous electrolytes [27,28], showing that fundamental investigations on the reaction mechanism must be intensified in AZBs [3,10,11]. The few already published papers only focus on the 2 electron-reaction, carried out in 3 mol L^{-1} $ZnSO_4$ or $Zn(CF_3SO_3)_2$ aqueous electrolytes, leading to scattered capacity values in the range 220-470 mAh g^{-1} [27,28]. Although the structural mechanism has not been completely solved, zinc and water insertion are thought to be responsible for the formation of a $Zn_xV_2O_5$, nH_2O compound upon the first discharge. After an activation process over a few or a few dozen of cycles, a highly stable capacity can be reached.

Recently, some of us proposed the use of a novel aqueous Zn/$LiFePO_4$ rechargeable battery using a binary concentrated electrolyte of 3 mol L^{-1} LiCl and 4 mol L^{-1} $ZnCl_2$ at an optimized pH 4 ensuring high conductivity and electrodes stability [29]. Remarkable cycling performance were obtained with a capacity of 92 mAh g^{-1} over 400 cycles at 6 C as well as a high rate capability with still 72 mAh g^{-1} available at 30 C. This original concept of binary electrolyte with both zinc and lithium ions has never been applied to the Zn/V_2O_5 system. It relies on a high ionic conductivity with sufficient amounts of zinc on one side for efficient cyclability of zinc anode and of lithium on the other side for reversible insertion/extraction in the host cathodic material. These appealing results prompted us to evaluate the Zn/V_2O_5 system in the binary lithium-zinc aqueous electrolyte at optimized pH 4.

In the present work, we report the electrochemical properties of V_2O_5 in 3 mol L^{-1} Li_2SO_4 - 4 mol L^{-1} $ZnSO_4$ electrolyte in the 1.6 V - 0.8 V vs. Zn^{2+}/Zn voltage window, with special attention paid to the structural mechanism involved upon the discharge-charge process and cycling. We show that V_2O_5 exhibits a similar discharge-charge profile in this binary aqueous

electrolyte than in non-aqueous lithiated electrolyte. Promising performance are outlined, with a highly reversible behavior and capacity values varying from 140 mAh g^{-1} at low rate to 80 mAh g^{-1} at 1 C. At 1 C rate, the capacity retention is, with a faradic efficiency of 100%, excellent over more than 300 cycles. X-ray diffraction coupled with Raman spectroscopy is carried out on discharged and charged electrodes to provide initial insights into the mechanism: a highly reversible lithiation-delithiation process is revealed. Furthermore, we demonstrate the structure changes of V_2O_5 in aqueous electrolyte have a mitigated amplitude compared to those usually displayed in non-aqueous LIBs, probably due to the co-insertion of zinc ions by the end of the reaction.

Experimental

V_2O_5 powder (Alfa Aesar, 99,5%) was used as received. Electrochemical studies were carried out in two-electrode split cells (MTI Corporation) where a zinc disk (Goodfellow) with 14 mm diameter acts as reference and auxiliary electrode. The positive electrode was prepared by mixing 90 wt% of V_2O_5, 6 wt% polyvinylidene fluoride (PVdF, Kynar, HSV900) as a binder and 4 wt% ketjen black (Ketjen Black International Co., Japan) as a conducting agent in 1-methyl-2-pyrrolidinone (NMP, Sigma-Aldrich). The resultant slurry was coated on a carbon paper (Alfa Aesar Co.), vacuum dried at 70 °C for 2 h and cut into disks 8 mm in diameter. The active material loading in the electrodes was about 2.5-3.2 mg. The electrolyte was prepared by dissolving 3 mol L^{-1} Li_2SO_4 and 4 mol L^{-1} $ZnSO_4$ in deionized water and the pH was adjusted to 4. A AGM (Absorptive Glass Mat NSG Corporation) separator was soaked with 80 µL of the resultant electrolyte and used in the battery. The two-electrode cells were tested galvanostatically at various C rates (1 C corresponds to 147 mA g^{-1}) and by cyclic voltammetry (sweep rate 0.2 mV s^{-1}), using a VMP3 Bio-Logic apparatus. The tests temperature was controlled and maintained at 20 °C. All potentials are reported in V vs. Zn^{2+}/Zn and specific capacities per gram of active material.

In order to investigate the structural mechanism involved upon the discharge-charge process of V_2O_5 in aqueous binary electrolyte, the cells were discharged to the required composition by galvanostatic reduction at C/5 rate. A C/20 rate was used to reach the highest depth of discharge. After 1h equilibrium, the electrodes were removed from the cell in the air and rinsed with water to remove all traces of salts. The X-Ray Diffraction (XRD) experiments were performed using a PANalytical X-Pert Pro diffractometer equipped with a X'celerator

linear detector and Co Kα source. Data are then processed on Eva software to identify peaks and adjusted the cell parameters of the identified phases. The Raman spectra were measured with a LaBRAM HR 800 (Jobin-Yvon-Horiba) Raman micro-spectrometer including Edge filters and equipped for signal detection with a back illuminated charge coupled device detector (Spex CCD) cooled by Peltier effect to 200 K. A He:Ne laser (632.8 nm) was used as the excitation source. The spectra were measured in back-scattering geometry. The resolution was about 0.5 cm^{-1}. A 100× objective was used to focus the laser light on sample surface to a spot size of 1 μm^2. To avoid local heating of the sample, the power of the laser beam was adjusted to 0.2–0.5 mW with neutral filters of various optical densities. Raman spectra were recorded on ten different spots of each electrode to check the homogeneity. This led to similar spectra for all the investigated points, whatever the composition.

Energy dispersive X-ray (EDS) analysis (accelerating energy of 20 keV) was applied to determine the elements in the electrodes together with electron microscopy (Zeiss, Merlin-type microscope).

Results and discussion

The storage behavior of V_2O_5 in aqueous binary electrolyte, 3 mol L^{-1} Li_2SO_4 and 4 mol L^{-1} $ZnSO_4$, is investigated in the 1.6 V- 0.8 V voltage window (**Figs. 1a-1b**). The voltammetric curve performed at 0.2 mV s^{-1} displays two-well defined cathodic peaks located at 1.12 V and 0.91 V. The anodic scan reveals a quantitative rechargeability (**Fig. 1a**). A broad current peak is observed, with two contributions at 1.21 V and 1.33 V corresponding to the second and first cathodic peaks, respectively. The discharge-charge profile of V_2O_5 at C/5 rate (**Fig. 1b**) highlights two distinct reduction steps at 1.16 V and 0.95 V involving a total faradaic yield of 0.87 F mol^{-1}. A symmetric charge process shows a reversible mechanism with two steps at 1.03 V and 1.21 V. This rechargeable behavior leads to a specific capacity of 128 mAh g^{-1} and calls for several comments. First, the electrochemical fingerprint in aqueous medium strongly resembles the typical V_2O_5 galvanostatic cycle in non-aqueous lithiated electrolyte with two well-defined plateaus separated by ca. 200 mV and involving quite the same reversible specific capacity [30]. Second, cyclic voltamperograms registered in aqueous electrolytes containing single lithium salt, single zinc salt and both (**Fig. 2a**) enlighten us on the electronic reactions likely to occur. Indeed, a first reduction step is observed at 1.12 V with the two electrolytes containing Li_2SO_4 while it is not present when single $ZnSO_4$ is used.

Then, it is reasonable to assume that lithium ions are first selectively inserted in binary electrolyte. At lower potential, reduction curves obtained with the three electrolytes exhibit a peak around 0.92-0.94 V, giving piece of evidence that both lithium and zinc insertion can take place at this potential. In addition, the comparison of cyclability during cycling in electrolytes containing only the lithium salt or containing both lithium and zinc salts (**Fig. 2b**) highlights the merit of the hybride electrolyte. Indeed, the available capacity decreases rapidly in the electrolyte without zinc while it is stable over 300 cycles in the electrolyte containing the 2 salts. These findings support the insertion of lithium ions previously suggested but leads to consider also a possible concomitant zinc insertion. This peculiar result prompted us to investigate the insertion mechanism of V_2O_5 in binary Li^+/Zn^{2+} electrolyte, using XRD and Raman spectroscopy.

The XRD patterns of discharged electrodes at C/5 as a function of the faradaic yield x expressed in F mol^{-1} ($0 \leq x < 1$) are gathered in **Fig. 3**. A lower C/20 rate was applied to reach the highest depth of discharge of 0.93. Before discharge, the pristine electrode exhibits the typical XRD pattern of V_2O_5 that can be indexed in an orthorhombic cell (space group *Pmmn*) with the following unit cell parameters: a = 11.49 Å, b = 3.56 Å, c = 4.36 Å (PDF 00-041-1426). Sharp and intense diffraction peaks indicate a high crystallization degree. The evolution of XRD patterns along the reduction process does not reveal strong modification since all the diffraction peaks of the V_2O_5 oxide are retained. However, examination of enlarged views in **Figs. 3b-3c** reveals a significant shift towards lower angles of the *001*, *101*, *011* and *111* lines while the *200*, *400* and *310* reflections slightly shift towards higher angles (**Figs. 3a-3c**). These trends indicate a decrease in the *a* parameter upon discharging, i.e. a contraction of the V-V distances in the V_2O_5 layers while at the same time the *c* parameter, i.e. the interlayer distance, increases. In addition to these changes, progressive broadening of the diffraction peaks gives evidence for a disordering process throughout the reduction. For $x \leq 0.3$, the enlarged views (**Figs. 3b-3c**) reveal a diphasic domain with two sets of *001*, *101*, *301* and *400* lines. Unit cell parameters reported in **Fig. 4** confirm the coexistence of the α-$Li_xV_2O_5$ phase (a = 11.49 Å; b = 3.56 Å; c = 4.38 Å) with a reduced phase (a = 11.42 Å; b = 3.57 Å; c = 4.47 Å) that can be assigned, considering the cell parameter values, to the lithiated ε-$Li_{0.3}V_2O_5$ phase reported in usual organic electrolyte [29]. This assignment to a lithiated V_2O_5 phase is perfectly consistent with the involved redox process previously proposed. Indeed, in the $0 \leq x \leq 0.3$ composition domain, the potential remains higher than 1.05 V,

where only the lithium ions are likely to be inserted in the material. For $0.3 < x \leq 0.93$, a single set of diffraction lines is observed depicting a solid solution behavior with a continuous contraction in *a* parameter and increase in *c* parameter to reach *a* = 11.35 Å and *c* = 4.58 Å for the fully discharged electrode (x = 0.93). This corresponds to a continuous lithium enrichment of ε-$Li_xV_2O_5$ up to the ε-$Li_{0.93}V_2O_5$ composition. The unit cell parameters values found for ε-$Li_{0.93}V_2O_5$ are in good accord with those previously reported for ε-$Li_{0.95}V_2O_5$ [31]. At this point, several comments are noteworthy: i) the *b* parameter keeps a quite constant value (*b* = 3.56-3.57 Å); ii) the composition range observed for the α-ε diphasic region matches that reported for non-aqueous electrolytes [30,32]; iii) the single-phase ε-$Li_xV_2O_5$ behavior strongly contrasts with the diphasic ε-$Li_{0.5}V_2O_5$/δ-LiV_2O_5 region usually reported in organic electrolytes [30,32]. In the present case, the structural impact of the reduction process leads to a very moderate increase in the unit cell volume that does not exceed 4 % (**Fig. 4b**). This low magnitude of variations discards any hypothesis of water insertion while the insertion reaction of lithium ions has been highlighted. However, at the stage of the study, a possible involvement of a few Zn^{2+} ions cannot be definitively excluded to explain the peculiar structural response of V_2O_5 upon discharging.

Raman spectroscopy experiments have also been carried out to investigate the structural impact of the reduction at the scale of the chemical bond. Raman spectra obtained at different depths of discharge are shown in **Fig. 5**. From a spectroscopic viewpoint, the point symmetry group of V_2O_5 crystal is D^{13}_{2h} and the Raman spectrum of the pristine material exhibits the typical V_2O_5 fingerprint, consisting in 10 peaks located at 105, 146, 199, 286, 305, 406, 483, 529, 703 and 994 cm^{-1}. Most of the low wavenumber modes can be described in terms of external modes of V_2O_5 units. They have been derived from relative motions of two V_2O_5 units belonging to the unit cell, three of them generating displacements of vanadium atoms along *x* axis (199 cm^{-1}), *y* axis (146 cm^{-1}) and *z* axis (105 cm^{-1}). Internal modes on the other hand, which are observed in the medium and high wavenumber region, can be described in terms of V-O-V stretching modes. The band at 994 cm^{-1} is assigned to the V-O stretching vibration mode along *z* axis, corresponding to the shortest V=O vanadyl bond oriented along the *c* axis. The V-O-V stretching modes along *x* and *y* axis are observed at 529 cm^{-1} and 703 cm^{-1} respectively [30,31,33]. For x = 0.1, a new band at 982 cm^{-1} is observed in the V-O stretching vibration region, typical of the presence of V^{4+} ions. This band belongs to the Li-poor ε-$Li_xV_2O_5$ phase that coexists with V_2O_5 in the $0.1 \leq x \leq 0.3$ composition domain and is pure for x = 0.5. Indeed, the Raman spectrum recorded for x = 0.5

exhibits the characteristic lines of ε-$Li_{0.5-0.6}V_2O_5$ at 158, 475, 421, 536, 707 et 983 cm^{-1} [34]. For $0.5 \leq x \leq 0.93$, further Li accommodation in the ε-phase induces a strong intensity decrease in the band at 158 cm^{-1} as well as a progressive broadening and shifts of typical bands: 475 cm^{-1} to 438 cm^{-1}; 707 cm^{-1} to 712 cm^{-1}; 536 cm^{-1} to 531 cm^{-1}; 983 cm^{-1} to 977 cm^{-1}. In addition, a new feature at 957 cm^{-1} can be detected for x = 0.93. The Raman spectrum of the fully discharged electrode (x = 0.93) matches that previously reported for the Li-rich ε-LiV_2O_5 phase [28,33]. It is worth noting the typical fingerprint of the δ-LiV_2O_5 phase, characterized in particular by a sharp Raman band at 1008 cm^{-1} [30,34], is not observed.

These findings are in good agreement with those deduced from the XRD study and outline a specific structural behavior in binary aqueous electrolytes. Indeed, both XRD and Raman investigations do not detect the formation of the folded δ-LiV_2O_5 phase in Li^+/Zn^{2+} electrolyte.

A minor participation of zinc ions has therefore to be considered, in good accordance with EDS analysis giving around 0.02 Zn per V_2O_5, as zinc insertion reaction into V_2O_5 is reported to occur in the potential range 0.9 - 1 V (**Fig. 2a**). In this scenario, the inserted Zn^{2+} cations located between the oxide layers would act as pillar species, then hindering the gliding of one layer over two in the *b* direction leading to the corrugated δ-phase.

However, the stabilization of the architecture afforded by the presence of Zn^{2+} ions is not a mandatory condition for the δ-phase not to appear. Indeed, another example of mitigated structural changes was recently reported for nanosized V_2O_5 [35]. In that case, it was demonstrated that the nanosized effect prevents the emergence of the distorted δ-LiV_2O_5 phase to the benefit of a solid solution behavior throughout the reduction process ($0 < x < 1$) [35]. Conversely, P. G. Dickens claimed to form the δ-LiV_2O_5 as the final product of V_2O_5 reduction in an aqueous LiCl electrolyte but without producing the corresponding XRD pattern [36]. To check whether zinc is responsible for the moderate structure changes of the V_2O_5 host lattice highlighted in this work, a V_2O_5 electrode was deeply discharged at x = 0.9 in a single salt aqueous 3 mol L^{-1} Li_2SO_4 electrolyte. In that case, the corresponding XRD pattern (**Fig. 6a**) and the Raman spectrum (**Fig. 6b**) show unambiguously the formation of the δ-LiV_2O_5 phase. Indeed, the X-ray diffractogram exhibits two sets of peaks: those characteristic of ε-LiV_2O_5, with parameters a = 11.38 Å, b = 3.57 Å and c = 4.59 Å, and a second set ascribed to the δ-LiV_2O_5 phase (orthorhombic cell, *Amam* space group) with

parameters a = 11.24 Å, b = 3.60 Å and c = 9.90 Å (JCPDS file 04-010-2882 [35]). Consequently, in δ-LiV_2O_5 phase, the interlayer distance corresponds to $c/2$ i.e. 4.95 Å against 4.58 Å for the present fully discharged compound ε-$Li_{0.93}V_2O_5$ (**Fig. 4a**).

Raman spectroscopy investigation confirms the formation of δ-LiV_2O_5 at the atomic scale in single salt Li_2SO_4 electrolyte. Indeed, the Raman spectrum (**Fig. 6b**) exhibits the characteristic bands of the δ-phase at 91, 152, 180, 252, 289, 420, 433, 631, 670 and 1007 cm^{-1} [30,34], in mixture with the Li-rich ε-$Li_{0.9-1}V_2O_5$ phase (bands at 708, 958 and 978 cm^{-1}).

These whole findings demonstrate the V_2O_5 discharge process in the Li_2SO_4-$ZnSO_4$ binary electrolyte involves a lithiation mechanism very likely associated to the co-insertion of a few Zn^{2+}. Zinc cations would act as pillar species preventing important structural changes usually observed at the end of the discharge in non-aqueous electrolyte, like the gliding of one oxide layer over two in the *b* direction.

Fig. 7a shows the cycling performance of V_2O_5-Zn battery using binary electrolyte at 1 C in the 1.6 V – 0.8 V voltage window. An attractive capacity of 80 mAh g^{-1} is obtained in this narrow voltage range without any capacity fading over 300 cycles (inset in **Fig. 7a**). In addition, the voltage profile is almost not affected upon cycling. These results suggest an excellent structural reversibility, a high stability of the cathode material in the binary electrolyte and no dissolution process. **Figs. 7b** and **7c** give evidence for the high reversibility of the structural mechanism previously described. Comparison of Raman spectra of the cathode material before cycling, after 1 cycle and after 300 cycles at 1 C clearly demonstrates the total restoration of the host lattice at the atomic scale, the Raman spectra of cycled electrodes perfectly matching that before cycling. Examination of the XRD patterns (**Fig. 7b**) shows that the structure of the pristine material is fully recovered at the end of the first cycle. In addition, the symmetric charge profile associated with a 100% coulombic efficiency makes no doubt the same electrochemical and structural mechanism is involved upon discharge and charge. However, after 300 cycles, α-V_2O_5 is found to coexist with traces of ε-$Li_xV_2O_5$ and an additional $Zn_3(VO_4)_2(H_2O)_3$ phase (JCPDS 04-018-46-01) [38]. The cell parameters of the ε-$Li_xV_2O_5$ phase (a = 11.46 Å, b = 3.56 Å, c = 4.46 Å) correspond to a low lithium content in ε-phase (**Fig. 4a**). This result proves that most of the lithium ions have been extracted from the interlayer spacing. On the other hand, the structure of the $Zn_3(VO_4)_2(H_2O)_3$ phase does not

correspond to an insertion compound belonging to the vanadium oxide family. This result highlights that the mechanism occurring upon cycling in the binary aqueous electrolyte is far from the one described when single zinc salt is used, leading to the formation of layered $Zn_xV_2O_5$, nH_2O [4,27], nor to the one occurring in pure aqueous Li electrolyte, involving the δ-LiV_2O_5 phase. Further work is required to examine in detail the reaction mechanism upon long term cycling.

The rate capability of the system has also been evaluated (**Fig. 7d**). The specific capacity delivered by commercial V_2O_5 in Zn-V_2O_5 hybrid battery of 110 mAh g^{-1} at C/5, decreases to 95, 85, 70, 45 and 25 mAh g^{-1} at C/2, 1 C, 2 C, 5 C and 10 C respectively. However, after cycling at a high rate of 10 C or 20 C, the initial capacity of 110 mAh g^{-1} can be recovered at C/5, showing no irreversible damage and the excellent structural stability.

Conclusion

A novel Zn-V_2O_5 aqueous rechargeable battery has been proposed, using a Li^+/Zn^{2+} binary electrolyte at pH 4. This cell exhibits a highly reversible capacity of 136 mAh g^{-1} at C/20 and 125 mAh g^{-1} at C/5 in the 1.6 V - 0.8 V range. In addition, an outstanding stability of the rechargeable capacity is observed, with 80 mAh g^{-1} available at 1 C and 100% capacity retention over 300 cycles. The discharge-charge profile achieved in aqueous medium is similar to that observed for the analogue reaction in organic lithiated electrolyte. However, an original reversible insertion mechanism isrevealed by XRD and Raman spectroscopy. Exclusive Li insertion in V_2O_5 occurs up to mid-discharge while the co-insertion of a few zinc ions is very likely involved in the second part of the reduction. Moderate interlayer spacing expansion and limited layers puckering point to much lower structural stress in aqueous binary electrolyte. A pillaring effect of a few interlayer Zn^{2+} ions is suggested, that hinders the formation of the distorted δ-LiV_2O_5 phase. The final discharge product corresponds unambiguously to the ε-rich LiV_2O_5 phase while the charge process ensures the quantitative extraction of cations, leading back to the pristine host lattice. The high structural stability of V_2O_5 even after 300 cycles makes this hybrid Zn/V_2O_5 system promising in aqueous binary electrolytes. Moreover, a significant rate capability improvement has already been evidenced using the same cathode material prepared by a nanosizing approach and will be soon presented in another research paper.

Acknowledgment

One of the authors wishes to thank the Ministry of Education and Science of Kazakhstan (grant number AP05136016-ZRABS), French Embassy in Astana, Kazakhstan and Campus France for financial support.

References

[1] J-M. Tarascon, M. Armand, Issues and challenges facing rechargeable lithium batteries, Nature 414 (2001) 359-367.

[2] H. Kim, J. Hong, K.-Y. Park, H. Kim, S.-W. Kim, K. Kang, Aqueous rechargeable Li and Na ion batteries, Chem. Rev. 114 (2014) 11788–11827.

[3] A. Konarov, N. Voronina, J.H. Jo, Z. Bakenov, Y.-K. Sun, S.-T. Myung, Present and future perspective on electrode materials for rechargeable zinc-ion batteries, ACS Energy Lett. 3 (2018) 2620–2640.

[4] D. Kundu, B.D. Adams, V. Duffort, S.H. Vajargah, L.F. Nazar, A high-capacity and long-life aqueous rechargeable zinc battery using a metal oxide intercalation cathode, Nat. Energy. 1 (2016) 16119.

[5] C. Xu, B. Li, H. Du, F. Kang, Energetic Zinc Ion Chemistry: The Rechargeable Zinc Ion Battery, Angew. Chemie Int. Ed. 51 (2012) 933–935.

[6] X.G. Zhang, Corrosion and electrochemistry of zinc, Springer Science & Business Media, 2013.

[7] N. Zhang, F. Cheng, Y. Liu, Q. Zhao, K. Lei, C. Chen, X. Liu, J. Chen, Cation-deficient spinel ZnMn2O4 cathode in $Zn(CF_3SO_3)_2$ electrolyte for rechargeable aqueous Zn-ion battery, J. Am. Chem. Soc. 138 (2016) 12894–12901.

[8] F.W.T. Goh, Z. Liu, T.S.A. Hor, J. Zhang, X. Ge, Y. Zong, A. Yu, W. Khoo, A near-neutral chloride electrolyte for electrically rechargeable zinc-air batteries, J. Electrochem. Soc. 161 (2014) A2080–A2086.

[9] H. Pan, Y. Shao, P. Yan, Y. Cheng, K.S. Han, Z. Nie, C. Wang, J. Yang, X. Li, P. Bhattacharya, Reversible aqueous zinc/manganese oxide energy storage from

conversion reactions, Nat. Energy. 1 (2016) 16039.

[10] J. Ming, J. Guo, C. Xia, W. Wang, H.N. Alshareef, Zinc-ion batteries: Materials, mechanisms, and applications, Mater. Sci. Eng. R Reports. 135 (2019) 58–84.

[11] G. Fang, J. Zhou, A. Pan, S. Liang, Recent Advances in Aqueous Zinc-Ion Batteries, ACS Energy Lett. 3 (2018) 2480–2501.

[12] M. Yan, P. He, Y. Chen, S. Wang, Q. Wei, K. Zhao, X. Xu, Q. An, Y. Shuang, Y. Shao, Water-lubricated intercalation in $V_2O_5{\cdot}nH_2O$ for high-capacity and high-rate aqueous rechargeable zinc batteries, Adv. Mater. 30 (2018) 1703725.

[13] P. He, Y. Quan, X. Xu, M. Yan, W. Yang, Q. An, L. He, L. Mai, High-Performance Aqueous Zinc-Ion Battery Based on Layered $H_2V_3O_8$ Nanowire Cathode, Small. 13 (2017) 1702551.

[14] T. Wei, Q. Li, G. Yang, C. Wang, High-rate and durable aqueous zinc ion battery using dendritic $V_{10}O_{24}{\cdot}12H_2O$ cathode material with large interlamellar spacing, Electrochim. Acta. 287 (2018) 60–67.

[15] F. Ming, H. Liang, Y. Lei, S. Kandambeth, M. Eddaoudi, H.N. Alshareef, Layered $Mg_xV_2O_5{\cdot}nH_2O$ as Cathode Material for High-Performance Aqueous Zinc Ion Batteries, ACS Energy Lett. 3 (2018) 2602–2609.

[16] B. Sambandam, V. Soundharrajan, S. Kim, M.H. Alfaruqi, J. Jo, S. Kim, V. Mathew, Y. Sun, J. Kim, $K_2V_6O_{16}{\cdot}2.7H_2O$ nanorod cathode: an advanced intercalation system for high energy aqueous rechargeable Zn-ion batteries, J. Mater. Chem. A. 6 (2018) 15530–15539.

[17] C. Xia, J. Guo, P. Li, X. Zhang, H.N. Alshareef, Highly Stable Aqueous Zinc-Ion Storage Using a Layered Calcium Vanadium Oxide Bronze Cathode, Angew. Chemie Int. Ed. 57 (2018) 3943–3948.

[18] V. Soundharrajan, B. Sambandam, S. Kim, M.H. Alfaruqi, D.Y. Putro, J. Jo, S. Kim, V. Mathew, Y.-K. Sun, J. Kim, $Na_2V_6O_{16}{\cdot}3H_2O$ barnesite nanorod: an open door to display a stable and high energy for aqueous rechargeable Zn-ion batteries as cathodes, Nano Lett. 18 (2018) 2402–2410.

[19] Z. Peng, Q. Wei, S. Tan, P. He, W. Luo, Q. An, L. Mai, Novel layered iron vanadate cathode for high-capacity aqueous rechargeable zinc batteries, Chem. Commun. 54

(2018) 4041–4044.

[20] T. Wei, Q. Li, G. Yang, C. Wang, An electrochemically induced bilayered structure facilitates long-life zinc storage of vanadium dioxide, J. Mater. Chem. A. 6 (2018) 8006–8012.

[21] B. Sambandam, V. Soundharrajan, S. Kim, M.H. Alfaruqi, J. Jo, S. Kim, V. Mathew, Y. Sun, J. Kim, Aqueous rechargeable Zn-ion batteries: An imperishable and high-energy $Zn_2V_2O_7$ nanowire cathode through intercalation regulation, J. Mater. Chem. A. 6 (2018) 3850–3856.

[22] G. Yang, T. Wei, C. Wang, Self-Healing Lamellar Structure Boosts Highly Stable Zinc-Storage Property of Bilayered Vanadium Oxides, ACS Appl. Mater. Interfaces. 10 (2018) 35079–35089.

[23] B. Tang, G. Fang, J. Zhou, L. Wang, Y. Lei, C. Wang, T. Lin, Y. Tang, S. Liang, Potassium vanadates with stable structure and fast ion diffusion channel as cathode for rechargeable aqueous zinc-ion batteries, Nano Energy. 51 (2018) 579–587.

[24] M.H. Alfaruqi, V. Mathew, J. Song, S. Kim, S. Islam, D.T. Pham, J. Jo, S. Kim, J.P. Baboo, Z. Xiu, Electrochemical zinc intercalation in lithium vanadium oxide: a high-capacity zinc-ion battery cathode, Chem. Mater. 29 (2017) 1684–1694.

[25] P. Hu, M. Yan, T. Zhu, X. Wang, X. Wei, J. Li, L. Zhou, Z. Li, L. Chen, L. Mai, Zn/V_2O_5 aqueous hybrid-ion battery with high voltage platform and long cycle life, ACS Appl. Mater. Interfaces 9 (2017) 42717-42722

[26] P. Hu, T. Zhu, J. Ma, C. Cai, G. Hu, X. Wang, Z. Liu, L. Zhou, L. Mai, Porous V_2O_5 microspheres: a high-capacity cathode material for aqueous zinc-ion batteries, Chem. Commun. 55 (2019) 8486-8489

[27] N. Zhang, Y. Dong, M. Jia, X. Bian, Y. Wang, M. Qiu, J. Xu, Y. Liu, L. Jiao, F. Cheng, Rechargeable Aqueous $Zn-V_2O_5$ Battery with High Energy Density and Long Cycle Life, ACS Energy Lett. 3 (2018) 1366–1372.

[28] J. Zhou, L. Shan, Z. Wu, X. Guo, G. Fang, S. Liang, Investigation of V_2O_5 as a low-cost rechargeable aqueous zinc ion battery cathode, Chem. Commun. 54 (2018) 4457–4460.

[29] N. Yesibolati, N. Umirov, A. Koishybay, M. Omarova, I. Kurmanbayeva, Y. Zhang, Y.

Zhao, Z. Bakenov, High Performance Zn/$LiFePO_4$ Aqueous Rechargeable Battery for Large Scale Applications, Electrochim. Acta. 152 (2015) 505–511.

[30] R. Baddour-Hadjean, A. Marzouk, J.P. Pereira-Ramos, R. Baddour-Hadjean, A. Marzouk, J.P. Pereira-Ramos, Structural modifications of $Li_xV_2O_5$ in a composite cathode ($0 \leq x < 2$) investigated by Raman microspectrometry, J. Raman Spectrosc. 43 (2012) 153–160.

[31] R. Baddour-Hadjean, C. Navone, J.P. Pereira-Ramos, In situ Raman microspectrometry investigation of electrochemical lithium intercalation into sputtered crystalline V_2O_5 thin films, Electrochim. Acta. 54 (2009) 6674–6679.

[32] C. Delmas, H. Cognac-Auradou, J.M. Cocciantelli, M. Menetrier, J.P. Doumerc, The $Li_xV_2O_5$ system - an overview of the structure modifications induced by the lithium intercalation, Solid State Ionics. 69 (1994) 257–264.

[33] M.B. Smirnov, E.M. Roginskii, K.S. Smirnov, R. Baddour-Hadjean, J.-P. Pereira-Ramos, Unraveling the Structure-Raman Spectra Relationships in V_2O_5 Polymorphs via a Comprehensive Experimental and DFT Study, Inorg. Chem. 57 (2018) 9190–9204.

[34] R. Baddour-Hadjean, E. Raekelboom, J.P. Pereira-Ramos, New Structural Characterization of the $Li_xV_2O_5$ System Provided by Raman Spectroscopy, Chem. Mater. 18 (2006) 3548–3556.

[35] D. Huo, A. Contreras, B. Laïk, P. Bonnet, K. Guérin, D. Muller-Bouvet, C. Cenac-Morthe, R. Baddour-Hadjean, J.P. Pereira-Ramos, Evidence for a nanosize effect on the structural and high performance electrochemical properties of V_2O_5 obtained via fluorine chemistry, Electrochim. Acta. 245 (2017) 350–360.

[36] P.G. Dickens, S.J. French, A.T. Hight, M.F. Pye, Phase relationships in the ambient temperature $Li_xV_2O_5$ system ($0.1 < x < 1.0$), Mater. Res. Bull. 14 (1979) 1295–1299.

[37] R.J. Cava, A. Santoro, D.W. Murphy, S.M. Zahurak, R.M. Fleming, P. Marsh, R.S. Roth, The structure of the lithium-inserted metal-oxide δ-LiV_2O_5, J. Solid State Chem. 65 (1986) 63–71.

[38] D.A. Hoyos, A. Echavarría, C. Saldarriaga, Synthesis and structure of a porous zinc vanadate, $Zn_3(VO_4)_2 \cdot 3H_2O$, J. Mater. Sci. 36 (2001) 5515–5518.

[39] N. Emery, R. Baddour-Hadjean, D. Batyrbekuly, B. Laik, Z. Bakenov, J.-P. Pereira-Ramos, B. Laïk, Z. Bakenov, J.-P. Pereira-Ramos, γ-$Na_{0.96}V_2O_5$: A New Competitive Cathode Material for Sodium-Ion Batteries Synthesized by a Soft Chemistry Route, Chem. Mater. 30 (2018) 5305–5314.

[40] I. Mjejri, A. Rougier, M. Gaudon, Low-Cost and Facile Synthesis of the Vanadium Oxides V_2O_3, VO_2, and V_2O_5 and Their Magnetic, Thermochromic and Electrochromic Properties, Inorg. Chem. 56 (2017) 1734–1741.

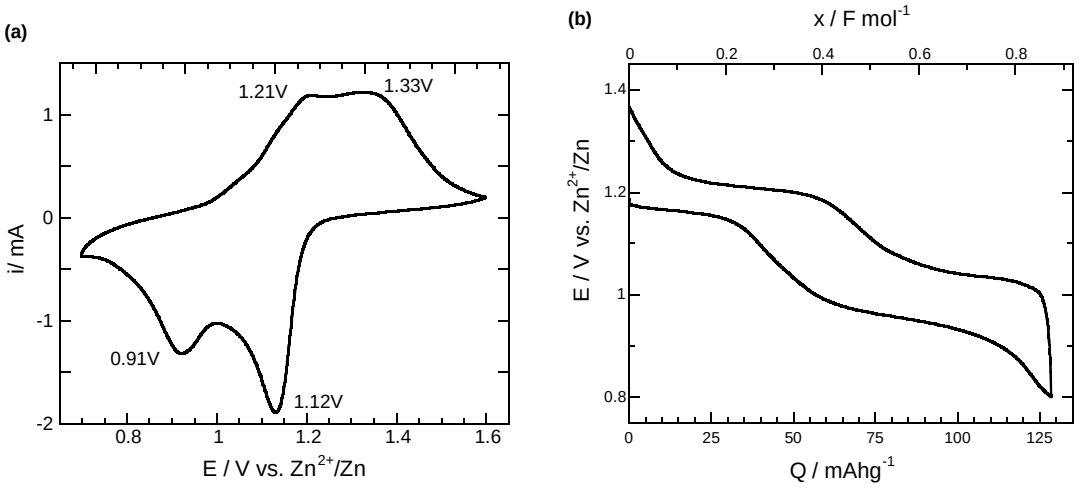

Figure 1: First (a) voltammetric and (b) galvanostatic cycles of a Zn/Li_2SO_4-$ZnSO_4/V_2O_5$ aqueous battery registered respectively at 0.2 mV s^{-1} and at C/5.

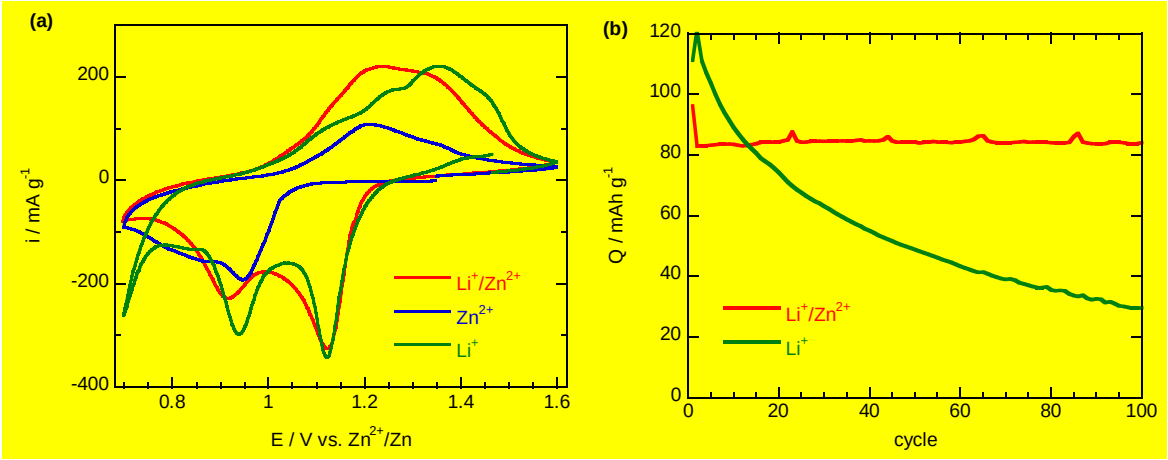

Figure 2: First (a) voltammetric cycles of Zn/3 mol L^{-1} Li_2SO_4- 4 mol L^{-1} $ZnSO_4/V_2O_5$ (red curve), Zn/3 mol L^{-1} Li_2SO_4/V_2O_5 (green curve) and Zn/4 mol L^{-1} $ZnSO_4/V_2O_5$ (blue curve) aqueous batteries registered at 0.2 mV s^{-1}. (b) Long-term cycling stability of Zn/3 mol L^{-1} Li_2SO_4- 4 mol L^{-1} $ZnSO_4/V_2O_5$ (red curve) and Zn/3 mol L^{-1} Li_2SO_4/V_2O_5 (green curve) aqueous battery at 1 C in the 1.6 V/0.8 V voltage range.

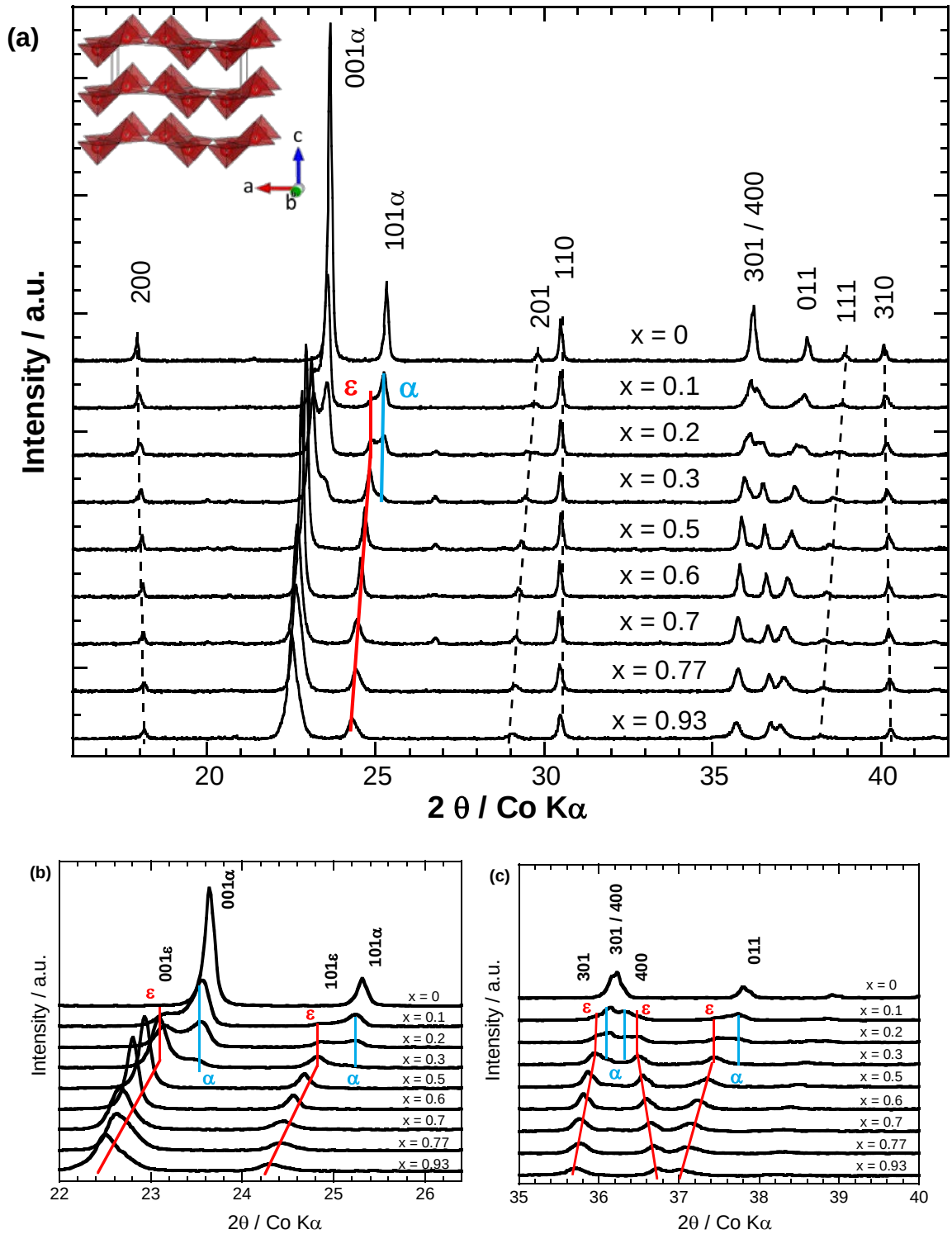

Figure 3: (a) X-ray diffraction patterns of reduced V_2O_5 electrodes for $0 \leq x \leq 0.93$. Zooms in the (b) 22 - 26.4° and (c) 35 - 40° 2θ ranges. α-$Li_xV_2O_5$ and ε-$Li_xV_2O_5$ peaks displacements during the first reduction process are shown schematically by blue and red lines respectively.

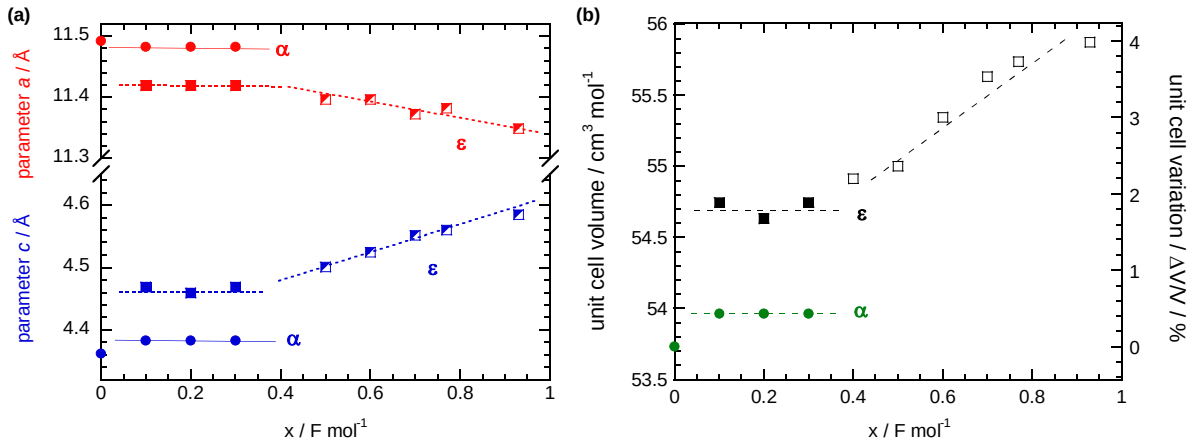

Figure 4: Evolution (a) of the unit cell parameters *a* (red) and *c* (bleu) and (b) of the unit cell volume as a function of x for 0 ≤ x ≤ 0.93 (circles and squares for α and ε phases respectively).

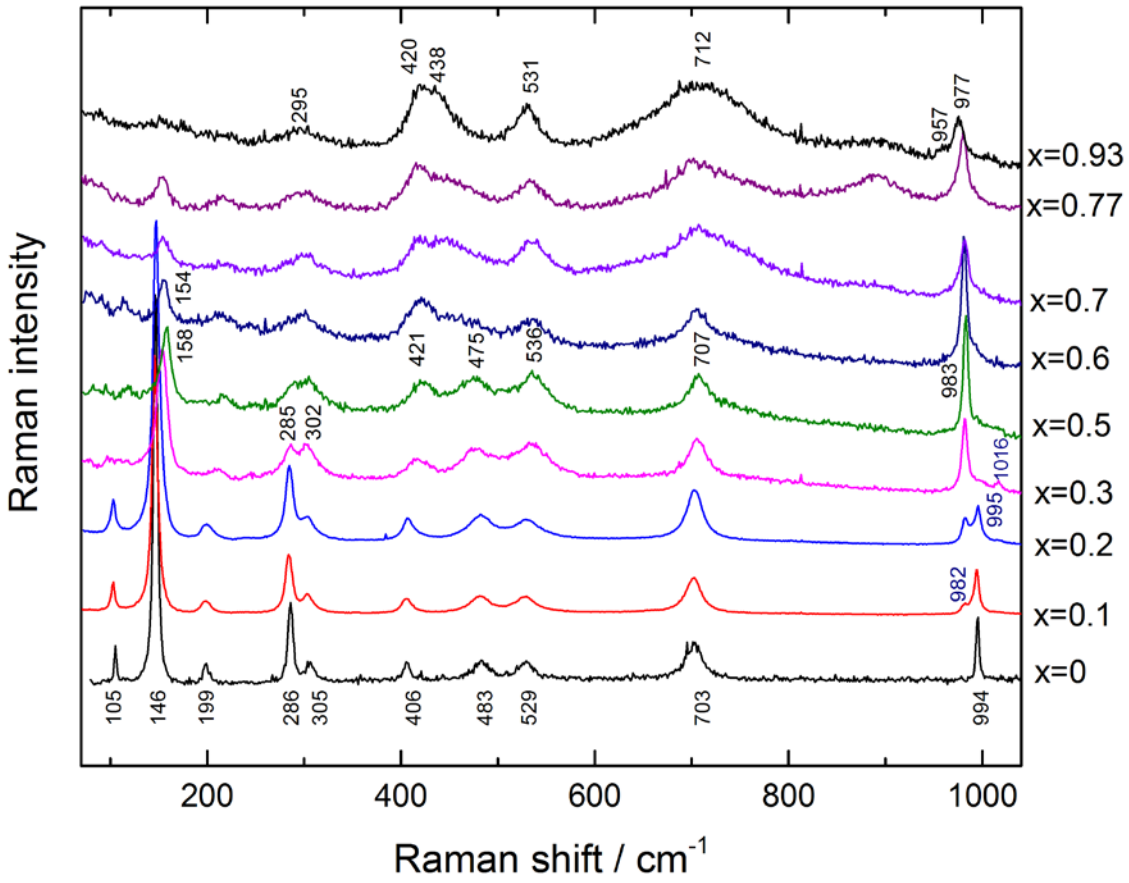

Figure 5: Raman spectra series collected on reduced V_2O_5 electrodes for 0 ≤ x ≤ 0.93 during the first discharge.

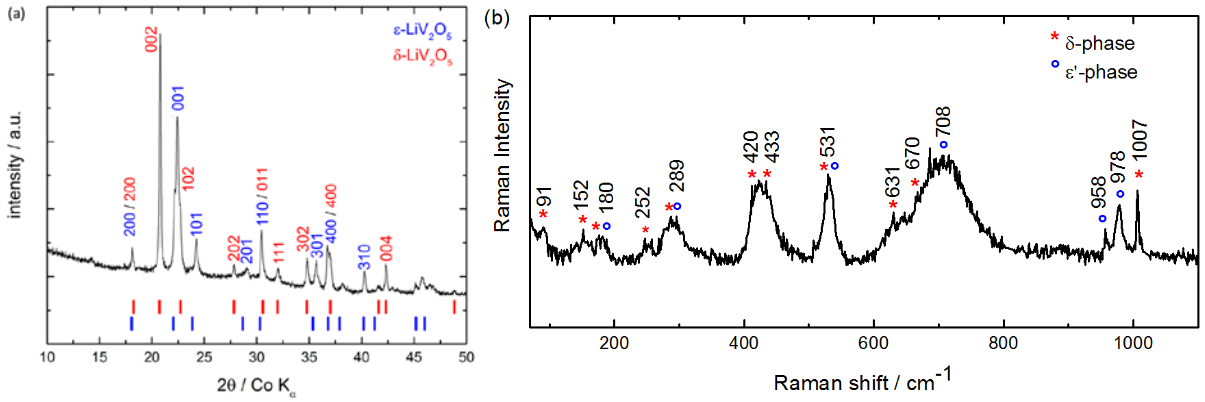

Figure 6: (a) X-ray diffraction pattern and (b) Raman spectrum of a V_2O_5 electrode reduced in 3 mol L^{-1} Li_2SO_4 electrolyte. C/20 rate. Cutoff voltage E = 0.8 V vs Zn/Zn^{2+} (x = 0.9 F mol^{-1})

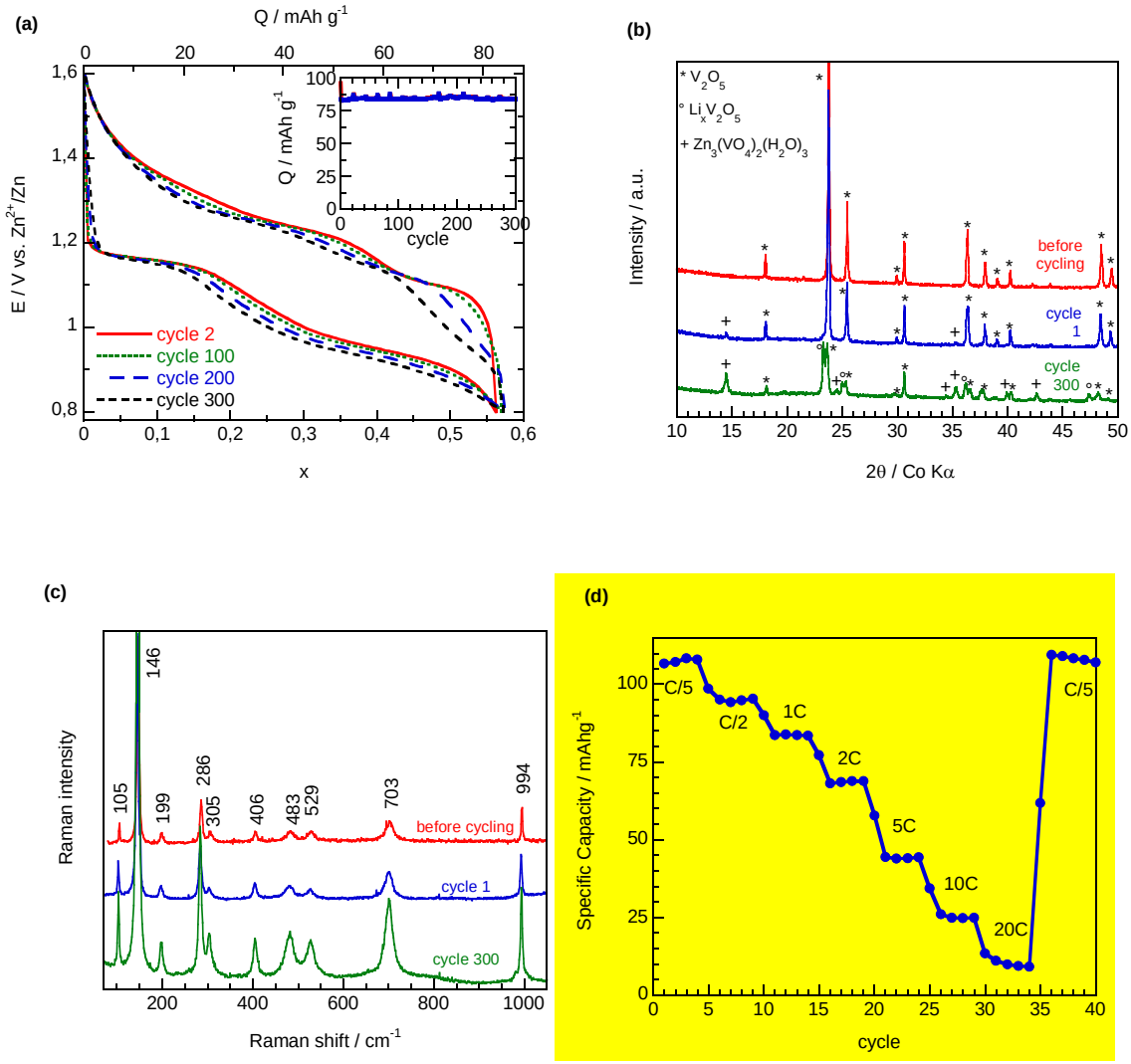

Figure 7: (a) Cycling performance and long-term cycling stability (inset) of V_2O_5 in the Zn/Li_2SO_4-$ZnSO_4$/V_2O_5 aqueous battery at 1 C in the 1.6 V/0.8 V voltage range. (b) X-ray diffraction patterns and (c) Raman spectra of the positiveV_2O_5 electrode before cycling and after a complete cycle (d) Rate capability at various current densities